Optical Properties of Sputtered SnS Thin Films for Photovoltaic Absorbers

Rona E. Banai, Hyeonseok Lee, Michael A. Motyka, Ramprasad Chandrasekharan, Nikolas J. Podraza, Jeffrey R. S. Brownson, and Mark W. Horn

***Abstract*—Tin monusulfide (SnS) is an absorber with promising optoelectronic properties and low environmental constraints of interest for high-efficiency solar cells. The optical properties of SnS thin films are investigated to assess their compatibility with the solar spectrum. SnS thin films were RF magnetron sputter-deposited at target powers of 105–155 W and total pressures of 5 to 60 mtorr in argon at room temperature. X-ray diffraction patterns confirmed a dominant tin monosulfide herzenbergite phase. The absorption coefficient was determined by spectroscopic ellipsometry and unpolarized spectrophotometry measurements. Both methods show that the films have absorption coefficients above the band gap in the range of 10^5–10^6 cm^{-1}. The direct gap, indirect gap, and forbidden direct gap for the films were found to be in the range of 1.2–1.6 eV, indicating a strong match with the solar irradiance spectrum.**

***Index Terms*—Absorption, ellipsometry, semiconductor materials, SnS, sputtering, thin films, tin compounds.**

I. Introduction

THE search for superior materials for solar cell applications is ongoing. While silicon-based solar cells dominate the market, production of thin-film photovoltaics (PV) is increasing. The increase is because of the potential for lower materials and production costs per module compared with the silicon modules [1]. Thin-film PV has the potential to support terawatt-level PV markets in the future. However, several manufacturability limitations including environmental concerns, raw material availability, and process scale-up constrain the long-term growth potential of incumbent devices that are based on CdTe or $Cu(In_{1-x}Ga_x)Se_2$ as the active layer. Materials without these limitations, with the potential to achieve high device efficiencies (>20%) required for PV to meet grid parity, must be investigated. Tin monosulfide (SnS) is one such material.

Manuscript received November 28, 2012; revised February 11, 2013; accepted February 22, 2013. Date of publication March 22, 2013; date of current version June 18, 2013. This work was supported by 3M.

R. E. Banai, H. Lee, J. R. S. Brownson, and M. W. Horn are with The Pennsylvania State University, University Park, PA 16802 USA (e-mail: rona@psu.edu; hxl250@psu.edu; nanomech@psu.edu; mhorn@engr.psu.edu).

M. A. Motyka was with The Pennsylvania State University, University Park, PA 16802 USA. He is now with Intel Mask Operations, Santa Clara, CA 95054 USA (e-mail: mamotyka00@gmail.com).

R. Chandrasekharan was with The Pennsylvania State University, University Park, PA 16802 USA. He is now as an energy consultant at VJ Coresoft Pvt. Ltd. in India (e-mail: ramprasad.c@gmail.com).

N. J. Podraza is with the University of Toledo, Toledo, OH 43606 USA (e-mail: Nikolas.Podraza@utoledo.edu).

Color versions of one or more of the figures in this paper are available online at http://ieeexplore.ieee.org.

Digital Object Identifier 10.1109/JPHOTOV.2013.2251758

SnS is natively p-type with ideal parameters for a solar cell absorber. SnS has a high absorption coefficient (α) of $\sim 10^5$ cm^{-1} above the band gap [2], a direct band gap of 1.21 eV, an indirect gap of 1.06 eV, and a high free-carrier concentration of around 10^{15} cm^{-3} [3]. Previous work in the literature has investigated several fabrication methods of SnS, such as electrochemical deposition [4], [5], sulfurization of tin thin films [6], thermal evaporation [3], [7], and sputtering [8]–[11]. SnS synthesis studies have focused on low-temperature processing techniques, preventing sulfur volatilization. However, wet chemistry techniques are generally not favorable for large-scale manufacturing of PV modules. Sputter deposition is known to produce high-quality films and is easily scalable but has not been explored sufficiently. A few studies have investigated sputtered SnS, but none have fully explored the parameter space [8]–[11]. Compositional, structural, and optical properties of sputter-deposited SnS thin films are reported here.

Despite the wide range of deposition methods that are used for SnS-based solar cells, the maximum efficiency achieved remains below 2% [12]. High series resistance, low shunt resistance, poor interface quality at the heterojunction, and low spectral response all contribute to the low maximum efficiency [12], [13]. A theoretical analysis of SnS|ZnO heterojunction PV solar cell was discussed in the work that was presented at the 38th IEEE Photovoltaics Specialists Conference [11]. The analysis showed that this device has the potential to achieve 20% efficiency. Through various characterizations of the thin-film materials, the model can be modified to better predict performance and speed up the process to produce high-efficiency devices.

The band gap and α of SnS has been reported for films produced by various deposition methods. The method to calculate α has not been consistent, reducing the ability to compare values. Analyses found in the literature have used several methods of determining α via first-order approximations [3], [7], [8]. The analysis presented here will elucidate why SnS is difficult to characterize optically, as well as why first-order approximations do not necessarily produce accurate representations of α.

One study used spectroscopic ellipsometry (SE) to determine the optical constants of nanocrystalline SnS. The optical models that were used to characterize the nanocrystalline SnS were B-spline fits [14]. This method fits wave bands separately and does not account for how the real and imaginary parts of the index of refraction are related via the Kramers–Kronig relation [15]. B-spline fits are convenient for getting an initial fit before using Kramers–Kronig consistent oscillator models, as was done here [15].

Both experimental and theoretical works show that SnS has an indirect and lowest direct band gap in the 1.0–1.5-eV range

[3], [5], [10], [13], [16]. The literature also shows that the zinc-blende phase of SnS has a forbidden direct band gap [17].

II. Methods and Materials

A. Sputter Conditions

SnS thin films were deposited in a radio-frequency (RF) magnetron sputtering system in a downward vertical geometry at room temperature. Target-to-substrate distance was 17 cm. Base pressures below 2×10^6 torr were achieved using a turbomolecular pump and measured with an ion gauge. Argon plasmas were ignited at 30–60 mtorr with the shutter closed, and then the shutter was opened for depositions at pressures ranging from 5 to 60 mtorr. Plasma power ranged from 105 to 155 W. Low pressures ($<$10 mtorr) were measured using an MKS cold cathode ion gauge, and higher pressures ($\geq$10 mtorr) were measured using an MKS Baratron gauge. The 3-in-diameter target used for these depositions was SnS of 99.999% purity (LTS Research Laboratories, Inc.). Films were deposited on silicon nitride-coated silicon wafers and glass microscope slides, simultaneously. Prior to deposition, substrates were cleaned using organic solvents. Deposition time was adjusted to control the film thickness. Colloidal graphite was painted in strips on substrates prior to deposition and was removed after deposition in an ultrasonic bath with isopropanol to facilitate profilometry measurements.

B. Compositional and Structural Characterization Methods

Several characterizations were conducted on SnS films. Film thickness was determined using a Tencor P-1 Long Scan Profiler. Composition was determined via Rutherford backscattering spectroscopy measurements (RBS, 1.7 MeV Tandetron Accelerator—located at Rutgers University). Surface morphology of the SnS films was assessed using the ZeissSMT1530, high-resolution field emission scanning electron microscopy (FESEM). SnS-phase analysis and structural properties were measured using glancing incidence X-ray diffraction (GIXRD) at an incident angle of 1° and detected from 5° to 70° (PANalytical X'Pert Pro MPD).

C. Optical Characterization Methods

Two methods were used to determine the absorption characteristics of the thin films. Transmittance and reflectance spectra were measured for SnS-coated glass slides using a Perkin Elmer Lambda 950 spectrophotometer over a spectral range from 300 to 2000 nm. The films were highly specular and reflection measurements were calibrated against spectra collected for an aluminum mirror.

If the reflectance R is zero, a first-order approximation of α is determined from film thickness d and transmittance T:

$$\alpha = -\frac{1}{d}\ln(T). \tag{1}$$

However, as the films have nonnegligible reflectance for the range of analysis, (1) cannot be used to approximate α. For films with high reflectance in the range of analysis, (2) must be used to determine α:

$$\alpha = -\frac{1}{d}\ln\left(\frac{T}{1-R}\right). \tag{2}$$

Both of these equations are found in the literature to determine α of SnS thin films.

SnS films less than 100-nm thick deposited on the silicon nitride-coated crystal silicon substrates were characterized using a multichannel, dual-rotating compensator spectroscopic ellipsometer [18] (model RC2, J.A. Woollam Co.) at 50°, 60°, 70°, and 80° over a spectral range of 0.75–5.15 eV. The ellipsometric spectra for these samples were analyzed using a structural model that consists of a semi-infinite crystal silicon substrate/silicon nitride layer/pre-sputtered SnS/bulk-SnS film/surface roughness/air ambient structure (CompleteEASE software, J.A. Woollam Co.). The optical constants of SnS thin films were modeled using Tauc–Lorentz oscillators [19], [20]. The optical properties of the surface roughness layer were represented with a Bruggeman effective medium approximation (EMA) consisting of 0.5 bulk-layer SnS and 0.5 void fractions. Similarly, the optical properties of the pre-sputtered SnS were represented with a Bruggeman EMA, with the void fraction set as a variable parameter. The unweighted error function between the experimental ellipsometric spectra and the model fit was less than 10^{-2}, with typical values less than 5×10^{-3}, indicating the validity of the optical and structural models. This analysis provided the SnS bulk-film thickness, surface roughness thickness, and the complex index of refraction ($N{=}n+ik$) for SnS, where n is the refractive index. The extinction coefficient k, determined from SE data, was used to calculate α with

$$\alpha = \frac{4\pi k}{\lambda} \tag{3}$$

where λ is the wavelength of light in centimeters.

Band gaps can be determined through the methods outlined by Pankove [21]. The allowed and forbidden direct band gap is found using

$$\alpha(h\nu) = A(h\nu - E_g)^n. \tag{4}$$

In this equation, the coefficient A is a constant, $h\nu$ is the photon energy, E_g is the band gap, and n is 1/2 or 3/2 for allowed and forbidden direct transitions, respectively. $(\alpha h\nu)^{1/n}$ is plotted against photon energy, and the most linear region extended to the x-axis will yield the band gap. Similarly, the indirect band gap is found using

$$\alpha(h\nu) = \frac{A'(h\nu - E_g - E_p)^2}{1-\exp\left(-E_p/kT\right)} \tag{5}$$

where A' is a different constant from A in (4), E_p is the phonon energy, and T is the temperature. E_g can be approximated using the same method as for finding the direct and forbidden gaps since $E_p \ll \mathrm{E}_g$. Additionally, disorder in the polycrystalline films buries the contributions of phonons near the band edge. To find the indirect band gap, $(\alpha h\nu)^1/2$ is plotted against photon energy and E_g is extracted from the most linear region.

TABLE I
SnS FILMS CHARACTERIZED IN THIS STUDY

Power (W)	Pressure (mTorr)	Thickness (nm)	Deposition Rate (nm/s)
105	5	130 ± 20	0.217 ± 0.038
105	60	69 ± 2	0.058 ± 0.003
105	60	250 ± 16	0.0463 ± 0.0031
115	10	240 ± 20	0.400 ± 0.041
135	5	224 ± 8	0.367 ± 0.020
135	60	80 ± 3	0.067 ± 0.007
155	5	320 ± 25	0.533 ± 0.051
155	60	77 ± 3	0.065 ± 0.005

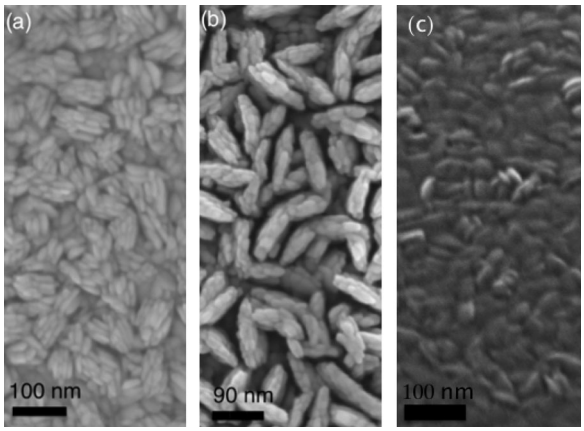

Fig. 1. Field emission scanning electron microscopy images of SnS material deposited at (a) target power 105 W, 5-mtorr total pressure; (b) target power 115 W, 10-mtorr total pressure; and (c) target power 105 W, 60-mtorr total pressure.

III. RESULTS AND DISCUSSION

Characterization of the SnS thin films in this study was two-fold: materials characterization to determine the structure and composition of the films, and optical characterization to determine the absorption properties of the active layer.

A. Compositional and Structural Characterization

To explore the impact of deposition parameters on film growth and microstructure, the impact of target power was studied for films deposited at different total pressures. Table I lists the deposition parameters, film thickness, and deposition rate of films characterized in this study. RBS measurements completed on samples with similar total pressures and target powers to the samples presented in Fig. 1 proved to have a nearly 1:1 ratio of SnS.

FESEM imaging of samples prepared under various deposition conditions shows significant changes in the shape, size, and density of the crystallites. Micrographs of films grown at 10 mtorr and varying powers showed little difference in the crystallite size and shape, indicating that for this pressure, power has little impact on the morphology [11]. Fig. 1 shows the impact of deposition pressure and target power on crystallite formation. These micrographs show that crystallite length increases and density decreases for the increase from 5 to 10 mtorr. However,

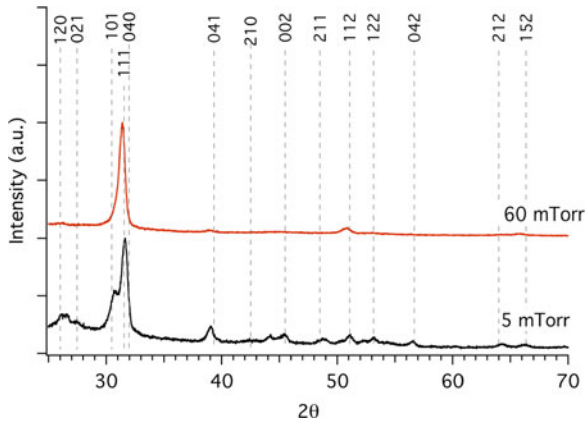

Fig. 2. X-ray diffraction patterns of SnS films deposited at 5- and 60-mtorr total pressure and 105-W target power. Pattern data are matched to PDF# 39–354.

as seen from Fig. 1(c), the high pressure gives a very dense film compared with the 5 and 10-mtorr samples. For an absorber layer in traditional planar PV devices, it is generally desirable to have large textured grains and densely packed crystallites with well-passivated grain boundaries. As more densely packed crystallites are produced at lower deposition rates and higher chamber pressures, these films are predicted to yield better performance in PV devices. The deposition parameter space must continue to be explored to produce larger crystallites.

X-ray diffraction patterns from the GIXRD measurements showed the primary phase of these films to be SnS. The pattern data best match PDF#39-354, which is herzenbergite SnS (Ortho; *Pbnm;* $2/m\ 2/m\ 2/m$; $a = 4.3291$, $b = 11.1923$, $c = 3.9838$, $Z = 4$). Fig. 2 shows the XRD patterns of two films deposited at 105 W, with one at 5 mtorr and the second at 60 mtorr. The atomic arrangement for herzenbergite can be found in [11]. No peaks were identified below 25°; therefore, these data were excluded. The films deposited at high pressure have preferential orientation in the (1 1 1) direction. Films deposited at low pressure have secondary inclusions of grains with (1 0 1) orientation, as well as, additional minor peaks of various orientations. It can be noted from Fig. 2 that peaks measured for these films do not exactly match the reference peak positions. This distortion is likely caused by strain in the film and variation of the lattice constant. Currently, steps are being taken to determine the cause of these peak shifts, and the full-width-half-maximum of these peaks is being used to determine film strain and crystallite size. One study by Nozaki *et al*. concluded that SnS films could have variable lattice parameters as a result of interfacial interaction between the film and the substrate [22]. For films of comparable thickness to those presented here, the lattice distortion continued through the film, perpendicular to the substrate [22]. Similarly, it is likely that interfacial effects between the film and the substrate cause the distortion seen in Fig. 2.

The data from Table I and Fig. 2 show that the film deposited at 5 mtorr had a high deposition rate but a more random distribution of crystallite orientations compared with the film deposited at 60 mtorr. The sample deposited at 60 mtorr had a slower deposition rate, but primarily one dominant orientation of crys-

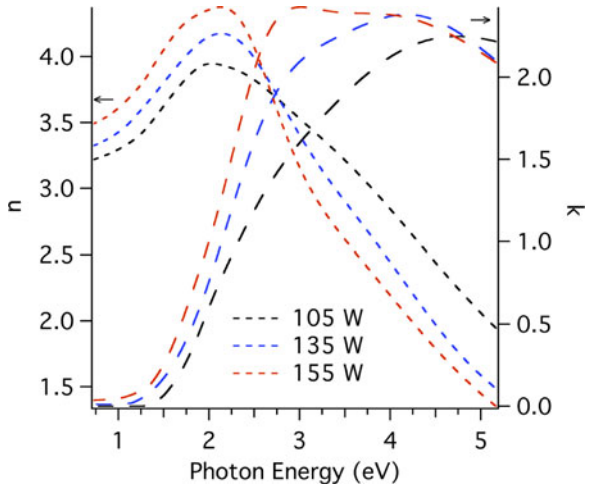

Fig. 3. Optical constants as derived from SE data. SnS was deposited at 60 mtorr total pressure.

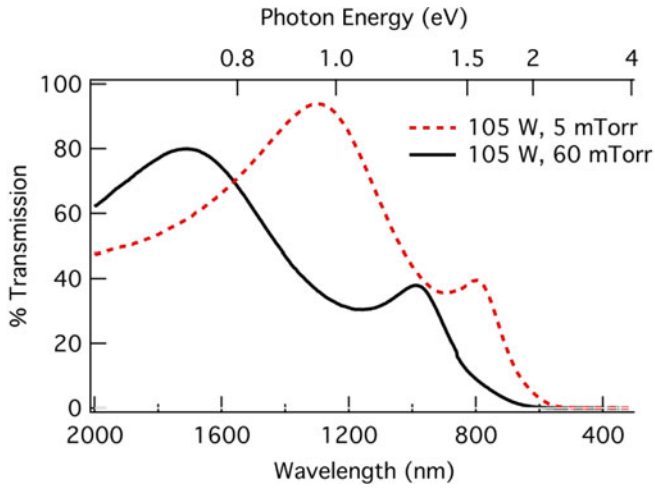

Fig. 4. Transmission spectra for SnS films grown (>100 nm) on glass slides.

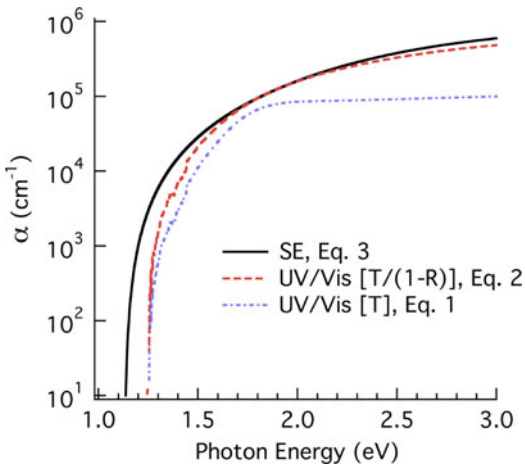

Fig. 5. Absorption coefficient (α) obtained from SE analysis and ultraviolet-visible spectrophotometry for an SnS film prepared at 135-W target power and 60 mtorr total pressure.

tallites. While the herzenbergite SnS matches most of the peaks in these X-ray patterns, the additional peaks suggest that another phase may be present in these films.

B. Optical Characterization

Optical constants n and k were determined for several samples using CompleteEASE software. Samples with varying target power and constant total pressure of 60 mtorr are shown in Fig. 3. As seen in this figure, k increases more rapidly for higher target power, indicating a sharper absorption onset. For higher powers, there is also a small peak that indicates a more pronounced direct energy transition. Additionally, n is increasing with increasing power below the absorption onset, indicating that the films deposited at higher power are denser. Higher density films are favorable for the absorber layer of a PV device because the minority carrier path lengths in such films may be longer than the optical absorption length. If the mean free path of carriers is limited by grain boundaries, more scattering events can occur, which shorten the path length. The shapes of n and k curves are comparable with the data found in the literature [23].

Fig. 4 shows the transmittance spectra obtained from spectrophotometry measurements of SnS films on glass slides. Fringes caused by coherent multiple reflections between substrate/film and film/ambient interface are observed for thicker films. The transmittance spectra for thinner films (< 50 nm) do not show interference fringes in the wavelength range shown in Fig. 4. In this case, the frequency of the interference pattern decreases with decreasing thickness, although coherent multiple reflections between interfaces still occur. These interference fringes have also been reported in the literature [7]–[9]. When the unpolarized transmittance and reflectance spectra of these SnS films are used in (1) or (2), the interference fringes appear as its artifacts in spectroscopic α, thus preventing accurate determination.

Fig. 5 shows spectroscopic α for a film prepared with a target power of 135 W and total pressure of 60 mtorr. Other very thin (<100 nm) SnS films produced at different sputtering conditions showed similar trends. As expected, when the reflectance is neglected, significantly different values of α are obtained, using (1). There is relatively good agreement between α extracted from SE and the combined analysis of transmittance and reflectance spectra at high energies. Near the band gap, the absorption coefficients diverge, indicating that the two methods might not find the same band gap. An absorption onset appears near 1.1–1.3 eV and reaches values $>10^5$ cm^{-1} by 1.6 eV. The high values of α and the absorption onset shown here indicate that SnS matches the solar irradiance spectrum well.

The direct, forbidden direct, and indirect gap for the samples grown at 60-mtorr total pressure and target power ranging from 105–155 W are listed in Table II in ascending order. Examples of how these band gaps were determined are shown in Fig. 6. The general trend shows the gaps to be consistent, regardless of the method used or target power. The trend shows the indirect gap to be 1.2–1.3 eV, the forbidden gap to be 1.3–1.34 eV, and the direct gap to be 1.47–1.55 eV. The major outlier is from the film produced at high target power as extracted from SE data. These trends show the gaps to be distinct from one another. These

TABLE II
BAND GAPS AND ABSORPTION ONSETS FOUND USING UV/VIS AND SE DATA FOR FILMS DEPOSITED AT 60 MTORR

Band Gap	Target Power (W)	Method	Value (eV)
Indirect	155	SE	1.10±0.01
Indirect	135	SE	1.21±0.01
Forbidden Direct	155	SE	1.23±0.02
Indirect	155	UV/Vis	1.24±0.01
Indirect	105	SE	1.27±0.01
Indirect	135	UV/Vis	1.27±0.03
Indirect	105	UV/Vis	1.30±0.01
Forbidden Direct	135	SE	1.30±0.02
Forbidden Direct	155	UV/Vis	1.32±0.01
Forbidden Direct	105	SE	1.33±0.02
Forbidden Direct	135	UV/Vis	1.33±0.02
Forbidden Direct	105	UV/Vis	1.34±0.03
Direct	155	SE	1.37±0.04
Direct	135	SE	1.47±0.05
Direct	155	UV/Vis	1.51±0.07
Direct	135	UV/Vis	1.51±0.09
Direct	105	SE	1.54±0.06
Direct	105	UV/Vis	1.55±0.08
E_g Parameter (Absorption onset) from SE	105	--	1.25±0.01
	135	--	1.15±0.03
	155	--	1.03±0.01

results match what is expected from Fig. 5. The discrepancy indicates that one or both methods that are presented here to determine that the band gap is insufficient. Since (2) is a first-order approximation, it is likely that it is insufficient because of multiple internal reflections in the thin film. Spectroscopic ellipsometry accounts for the internal reflections, resulting in a more accurate representation of the film's optical properties. It is also important to consider the fact that different substrates were used depending on the measurement type. Future work will entail spectrascopic ellipsometry of samples grown on glass.

To the authors' knowledge, the forbidden band gap has not been reported for herzenbergite SnS. According to the parity selection rule, the symmetry of the herzenbergite phase could cause the presence of a forbidden direct gap transition. Since the indirect band gap is at a lower energy than the forbidden gap, absorption is possible via the indirect transition.

Despite the films' lowest energy transition being indirect, the absorption coefficient of these films is comparable or better than thin film materials currently on the market. These results are promising for using SnS as an absorber material in a PV device. With high absorption, the material can be made thin, using less material to collect light. Additionally, minority carriers will be collected from the thin absorber before recombination events can occur.

IV. CONCLUSIONS AND FUTURE WORK

Sputtered SnS thin films are stoichiometric and primarily exhibit the herzenbergite phase. These thin films have small crystallites, which is generally nonideal for PV absorber layers.

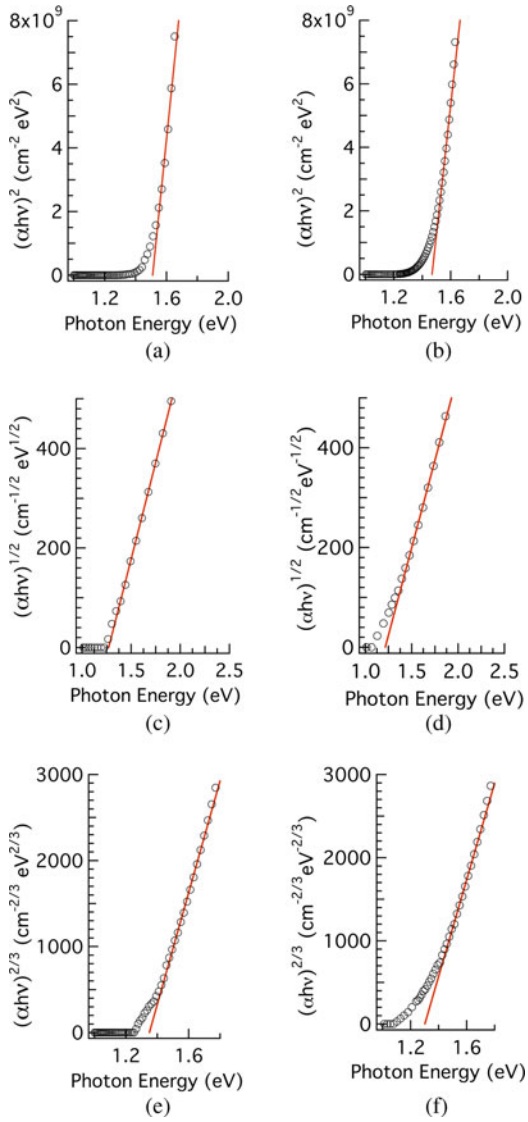

Fig. 6. Sample grown at 135-W target power and 60-mtorr total pressure. Direct band gap from (a) UV/Vis data (1.51 eV) and (b) SE data (1.47 eV); indirect band gap from (c) UV/Vis data (1.27 eV) and (d) SE data (1.21 eV); forbidden direct band gap from (e) UV/Vis data (1.33 eV) and (f) SE data (1.30 eV).

Sputtering conditions and postdeposition processing will need to be explored further in order to improve the crystallinity, grain size, and density of the SnS thin films.

Spectroscopic ellipsometry allows for the extraction of both n and k simultaneous to the determination of layer thicknesses in the sample but loses sensitivity to low values of α near $\sim 10^2$–10^3 cm^{-1}. Derivation of n and k showed how sputter deposition conditions affect film optical properties and density.

Optical characterizations showed SnS thin films to have spectroscopic $\alpha > 10^5$ cm^{-1} for energies greater than 1.5 eV, which is promising for its use as a PV absorber. Extraction of the direct, indirect, and forbidden direct band gaps was successful, and values are within the range quoted in the literature. The indirect gap of $\sim$1.3 eV is a strong match to the solar spectrum. Future work will repeat the analysis for films grown at other sputter conditions.

The authors postulate that the parity selection rule produces the forbidden direct gap in herzenbergite SnS. First, principle calculations of herzenbergite SnS will determine the orbitals of the valence and conduction bands. Once the orbitals are known, it can be determined if the parity selection rule applies to this phase of SnS.

The two methodologies that were used to determine the assessed α need not be exclusive of one another. Data from SE and unpolarized transmittance spectroscopy can be merged to yield highly accurate optical properties across the full spectral range. A rigorous analysis procedure merging the information will account for coherent multiple reflections present for film/substrate sample geometries. Future work will employ this method of analysis to better characterize and quantify the band gap of SnS films deposited on glass.

ACKNOWLEDGMENT

The authors would like to thank Dr. L. Wielunski at the Laboratory for Surface Modification at Rutgers University for completing RBS measurements and N. M. Wonderling (XRD), B. Jones (XRD), H. Basantani (RBS), J. Stapleton (spectrophotometry), and Y. Jin (profilometry) for their assistance with characterizations.

REFERENCES

[1] V. M. Fthenakis, H. C. Kim, and E. Alsema, "Emissions from photovoltaic life cycles," *Environ. Sci. Technol.*, vol. 42, no. 6, pp. 2168–2174, Mar. 2008.

[2] H. Noguchi, A. Setiyadi, H. Tanamura, T. Nagatomo, and O. Omoto, "Characterization of vacuum-evaporated tin sulfide film for solar cell materials," *Sol. Energy Mater. Sol. Cells*, vol. 35, no. 1–4, pp. 325–331, Sep. 1994.

[3] S. S. Hedge, A. G. Kunjomana, K. A. Chandrasekharan, K. Ramesh, and M. Prashantha, "Optical and electrical properties of SnS semiconductor crystals grown by physical vapor deposition technique," *Physica B*, vol. 406, pp. 1143–1148, Jan. 2011.

[4] S. Cheng, G. Chen, Y. Chen, and C. Huang, "Effect of deposition potential and bath temperature on the electrodeposition of SnS film," *Opt. Mater.*, vol. 29, pp. 439–444, Feb. 2006.

[5] J. R. S. Brownson, C. Georges, and C. Levy-Clement, "Synthesis of a delta-SnS polymorph by electrodeposition," *Chem. Mater.*, vol. 18, pp. 6397–6402, Dec. 2006.

[6] F. Jiang, H. Shen, W. Wang, and L. Zhang, "Preparation of SnS film by sulfurization and SnS/a-Si heterojunction solar cells," *J. Electrochem. Soc.*, vol. 159, pp. H235–H238, Jan. 2011.

[7] S. A. Bashkirov, V. F. Gremenok, and V. A. Ivanov, "Physical properties of SnS thin films fabricated by hot wall deposition," *Semiconductors*, vol. 45, pp. 765–769, Dec. 2010.

[8] A. Stadler and H. Dittrich, "Analysing UV/Vis/NIR spectra with the double-layer model—sputtered SnS thin-films II: Gas law and plasma parameter dependencies," *Thin Solid Films*, vol. 519, no. 19, pp. 6568–6578, Jul. 2011.

[9] W. Guang-Pu, Z. Zhi-Lin, Z. Wei-Ming, G. Xiang-Hong, C. Wei-Qun, H. Tanamura, M. Yamaguchi, H. Noguchi, T. Nagatomo, and O. Omoto, "Investigation on SnS film by RF-sputtering for photovoltaic application," in *Proc. IEEE 1st World Conf. Photovolt. Energy Conversion*, Waikoloa, HI, USA, 1994, pp. 365–368.

[10] K. Hartman, J. L. Johnson, M. I. Bertoni, D. Recht, M. Aziz, M. A. Scarpulla, and T. Buonassisi, "SnS thin-films by RF sputtering at room temperature," *Thin Solid Films*, vol. 519, pp. 7421–7424, Dec. 2010.

[11] R. E. Banai, H. Lee, M. Lewinsohn, M. A. Motyka, R. Chandrasakharan, N. J. Podraza, J. R. S. Brownson, and M. W. Horn, "Investigation of the absorption properties of sputtered SnS thin films," in *Proc. IEEE 38th Photovolt. Spec. Conf.*, Austin, TX, USA, 2012, pp. 164–169.

[12] K. T. Ramakrishna Reddy, N. K. Reddy, and R. W. Miles, "Photovoltaic properties of SnS-based solar cells," *Sol. Energy Mater. Sol. Cells*, vol. 90, no. 18–19, pp. 3041–3046, Nov. 2006.

[13] M. Devika, N. K. Reddy, K. Ramesh, R. Ganesan, K. R. Gunasekhar, E. S. R. Gopal, and K. T. Ramakrishna Reddy, "Thickness effect on the physical properties of evaporated SnS films," *J. Electrochem. Soc.*, vol. 154, no. 2, pp. H67–H73, Dec. 2007.

[14] E. R. Shaaban, M. S. Abd El-Sadek, M. El-Hagary, and I. S. Yahia, "Spectroscopic ellipsometry investigations of the optical constants of nanocrystalline SnS thin films," *Phys. Scr.*, vol. 86, no. 1, p. 015702, Jul. 2012.

[15] CompleteEASETM Data Analysis Manual, J. A. Woollam Co. Inc., Lincoln, NE, USA, 2009.

[16] J. Vidal, S. Lany, M. d'Avezac, A. Zunger, and A. Zakutayev, "Band-structure, optical properties, and defect physics of the photovoltaic semiconductor SnS," *Appl. Phys. Lett.*, vol. 100, no. 3, p. 032104, Jan. 2012.

[17] D. Avellaneda, M. T. S. Nair, and P. K. Nair, "Polymorphic tin sulfide thin films of zinc blende and orthorhombic structures by chemical deposition," *J. Electrochem. Soc.*, vol. 155, no. 7, pp. D517–D525, May 2008.

[18] C. Chen, I. An, G. M. Ferreira, N. J. Podraza, J. A. Zapien, and R. W. Collins, "Multichannel Mueller matrix ellipsometer based on the dual rotating compensator principle," *Thin Solid Films*, vol. 455, pp. 14–23, May 2004.

[19] G. E. Jellison, Jr. and F. A. Modine, "Parameterization of the optical functions of amorphous materials in the interband region," *Appl. Phys. Lett.*, vol. 69, no. 3, p. 371, Jul. 1996.

[20] G. E. Jellison Jr. and F. A. Modine, "Parameterization of the optical functions of amorphous materials in the interband region (erratum)," *Appl. Phys. Lett.*, vol. 69, no. 14, p. 2137, Sep. 1996.

[21] J. I. Pankove, *Optical Processes in Semiconductors*, 2nd ed. New York, USA: Dover, 1975.

[22] H. Nozaki, M. Onoda, M. Sekita, K. Kosuda, and T. Wada, "Variation of lattice dimensions in epitaxial SnS films on MgO(001)," *J. Solid State Chem.*, vol. 178, no. 1, pp. 245–252, Jan. 2005.

[23] R. Eymard and A. Otto, "Optical and electron-energy-loss spectroscopy of GeS, GeSe, SnS, and SnSe single crystals," *Phys. Rev. B*, vol. 16, no. 4, pp. 1616–1623, Aug. 1977.

Authors, photographs and biographies not available at the time of publication.